Lithology prediction through convolutional neural networks and rock physics-based synthetic wells: an example from Gulf of Mexico

Felipe Melo and Ruth Kurian, GeoSoftware

This paper was prepared for presentation during the 4th Joint SBGf/SEG Workshop on Machine Learning held in Rio de Janeiro, Brazil, 03-04 December 2024.

Abstract

Convolutional Neural Networks (CNNs) are used to predict lithology volumes by modeling the relationship between seismic angle gather data and well log data. The performance of this type of network is highly dependent on extensive training data which is often limited. To overcome this limitation, synthetic well data are generated from rock physics models and the statistical analysis of two real wells, systematically varying key reservoir parameters like porosity, reservoir layer thickness, and water saturation. These variations produce a range of scenarios that are not present in the input wells, but which may be present in the project area. This diverse set of synthetic wells along with corresponding synthetic angle gathers are used to train a CNN model for lithology prediction. To further refine the model, transfer learning is applied. After initial training on synthetic data, the CNN model is fine-tuned using data from just two real wells. Transfer learning improves the model's ability to capture local geological features, validated by agreement with lithology classifications from three blind wells. This study evaluates CNN models trained on synthetic data and validated using blind wells in the Middle Pliocene Gulf of Mexico's Mississippi Canyon Block 109. The results show geologically consistent lithology predictions and confirm the robustness of this approach.

Introduction

Volume lithology prediction from seismic data is of great significance for sweet-spot detection, reservoir delineation, and geologic model building (Xu et al., 2022). Traditionally, facies classification is performed with a Bayesian approach after deterministic inversion (Pendrel and Schouten, 2020). In recent years, machine learning has been used for lithology prediction. For example, Bekti (2020) performed facies classification on a field in the Gulf of Mexico using a Deep Feed-forward Neural Network classification model which showed agreement with Bayesian classification using deterministic inversion results.

Deep learning networks are highly dependent on sufficient labelled data to train and validate the results. Downton et al. (2020) proposed a hybrid theory-guided data science approach to overcome the issue of insufficient data and trained a deep neural network using synthetic well data to predict reservoir properties in a North Sea dataset. Allo et al. (2021) applied this workflow to characterize a carbonate geothermal reservoir. Downton et al. (2022) extended the hybrid theory-guided data science approach from Downton et al. (2020) to train a Convolutional Neural Network (CNN) to predict elastic and reservoir properties for the Barnett Shale, an unconventional field in USA. Colwell (2022) applied the same method to predict elastic and reservoir properties in the North Sea. Malik and Dixit (2022) used the same methodology to predict elastic and reservoir properties in Western Australia.

In this work, we follow the workflow proposed by Downton et al. (2022); however, instead of property prediction, we perform lithology prediction. We generate a set of synthetic well data from a rock physics model with systematic variations applied to two real wells. Then, the synthetic catalog is completed by applying the Zoeppritz equation to elastic logs, generating synthetic angle gathers from those wells. A CNN is initially trained with these data followed by transfer learning to integrate real data and fine tune the model. Finally, the model is applied to the seismic data to predict lithology throughout the seismic survey. The lithology prediction on a field in the Gulf of Mexico is validated in three blind wells and the resulting facies distribution is found to be geologically consistent.

Dataset

The study area is situated in the Mississippi Canyon Block 109, Gulf of Mexico and consists of sand and shale sequences. The depositional environment includes slumps, turbidites, prograding sandy mouth bars and a relatively undeformed upper slope area (Mayall et al., 1992).

The dataset is composed of time domain angle gathers, , ranging from 2 to 32 degrees. The interval of interest is between the Green and Blue horizons. There are five wells, with six well logs in each well. The selected well logs for this work are: Compressional Velocity (P-wave), Shear Velocity (S-wave), Density, Water Saturation (Sw), Volume of Clay (VClay) and Facies. Figure 1 shows Well 1 and the horizons overlaying the angle gather, on the left-hand side. The right-hand side of Figure 1 shows a full stack with the five wells and the two horizons over an arbitrary line. The test data (blind wells) for the facies prediction are Well 1, Well 2 and Well 3, highlighted in black in Figure 1.

The facies are described as Pay, Wet Shaly Sand and Shale, based on cutoffs of VClay and Sw. Figure 2 shows facies distribution on each well in the zone of interest. The distribution is unbalanced, where Shale is the dominant facies. In this work, we do not address the problem of unbalanced facies distribution.

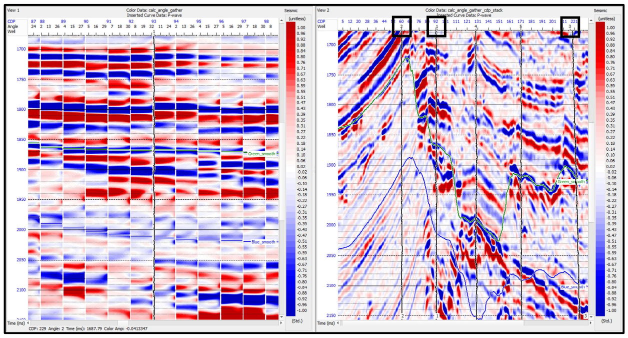

***Figure 1** – Seismic data. The angle gathers overlayed by Well 1 are displayed on the left-hand side. The full stack with an arbitrary line passing through all the wells is displayed on the right-hand side. The test wells are highlighted in black.*

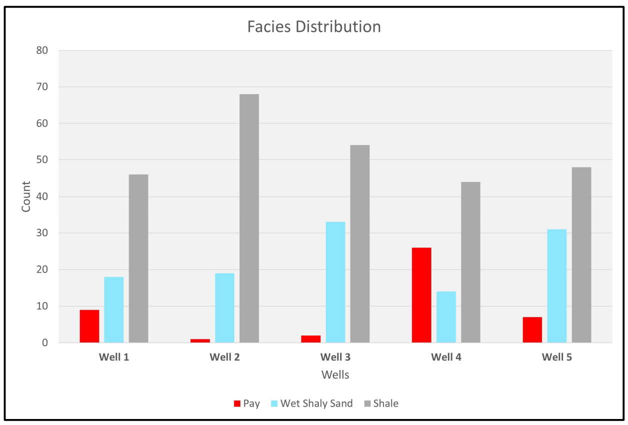

***Figure 2** – Facies distribution within the wells.*

Method

This work is divided into two main parts: generate the synthetic catalog and perform facies prediction through CNNs.

The main steps to generate the synthetic catalog are:

1) Litholayer Classification. We define and classify the lithology based upon cutoffs of the input curves. We use a two-step semi-supervised approach to automate this procedure. First, we classify each log sample into different lithology classes obtained based on a categorization of the VClay and Sw. In the second step, we agglomerate the thin lithology beds below a thickness threshold with adjacent beds sharing similar multivariate Gaussian statistics. Figure 3 shows the two input petrophysical logs for this step, three elastic logs for QC, the lithology log, and the resulting facies log (in the last track). The Pay facies is identified in red.
2) Rock Physics Model Calibration. In this work, a granular model that combines Hertz-Mindlin contact theory and Hashin and Shtrikman (1963) bounds is implemented. This model, which best describes unconsolidated (soft) sandstones (Dvorkin and Nur, 1996), was further extended to stiffer sandstones by Allo (2019) through the matrix stiffness index (MSI). To accurately estimate the measured logs, the RPM is calibrated by performing an inversion for the MSI. Figure 4 shows the measured, in orange, and computed logs, in blue, after this process in Well 5.

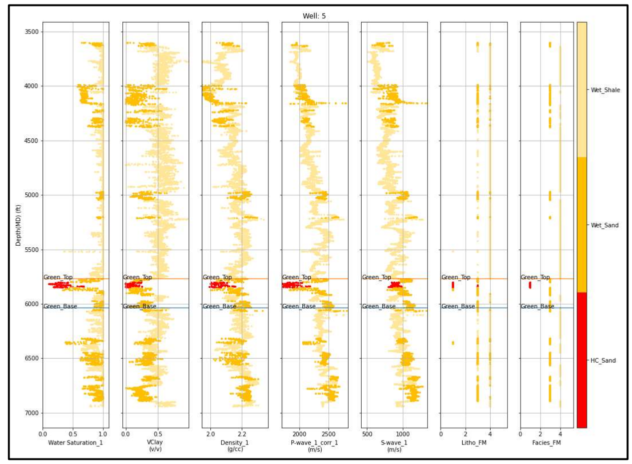

***Figure 3** – Litholayer classification in Well 5. Petrophysical properties (Sw and VClay) and elastic properties (Density, P-wave and S-wave) color coded by the lithofacies log. Lithology and Lithofacies logs are shown in the last two tracks. The Pay facies is identified in red.*

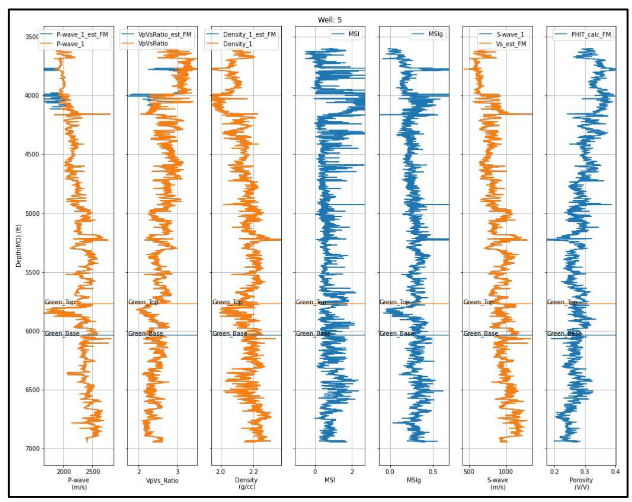

***Figure 4** – RPM calibration in Well 5. Input logs are displayed in orange and computed logs are displayed in blue.*

3) Well log statistics. For each lithofacies layer of step 1, we calculate the background trend and covariance matrix. In addition, we model the spatial correlation using an exponential variogram.
4) Simulations. Generating a series of pseudo-wells by simulating petrophysical logs based on the statistics determined in step 3. To ensure that the pseudo-wells sample the range of possible geologic scenarios, the thickness, porosity and water saturation of the reservoir layers were perturbed resulting in 270 pseudo wells. Then, the calibrated RPM from step 2 was used to generate the elastic properties from these petrophysical logs. Figure 5 illustrates the porosity

variations in Well 5 and their impact on other log data. The input logs are displayed in black and the simulated logs are displayed in blue.

5) Synthetic Generation. In the last step, synthetic angle gathers are generated for each pseudo-well using a convolutional model in which the P-wave reflection coefficients calculated using the Zoeppritz (1919) equations are convolved with a wavelet extracted from the real seismic data. Figure 6 shows a subset of the synthetic angle gathers generated from pseudo-wells. A synthetic p-wave is plotted in red in each angle gather.

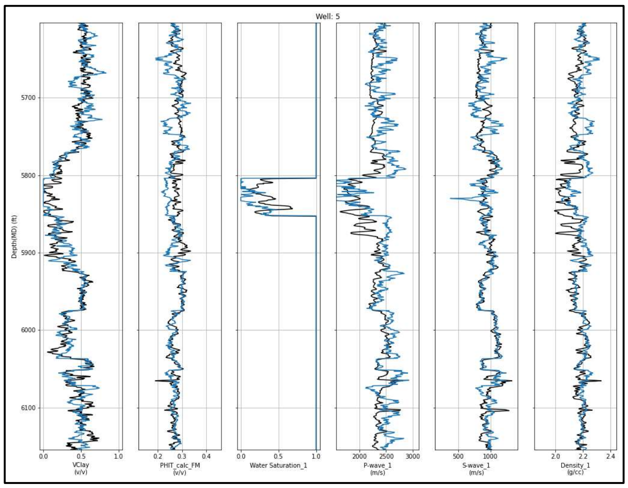

***Figure 5** – Systematic variation in Well 5. An example of porosity variations and their impact in other logs. The input logs are displayed in black and the simulated are displayed in blue.*

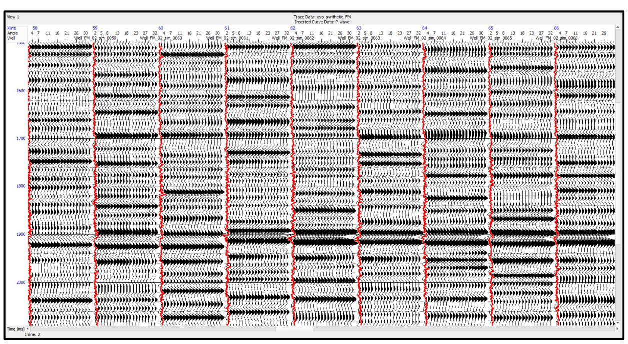

***Figure 6** – Subset of synthetic angle gathers generated from the pseudo-wells. A synthetic P-wave is plotted in red in each angle gather.*

In the second part, the CNN is trained using the pseudo-wells and seismic gathers. Then, the convolutional neural network operator is applied to the real data with transfer learning, and the classified facies are output as seismic volumes.

The main steps are:

1) CNN Training. The synthetic pseudo-wells and angle gathers are used to train the CNN. The data is divided into training and validation, where 70% of the wells are used for training and 30% for validation. In a high-level view, the architecture of the network is composed of two convolutional layers, each followed by a maximum pooling layer. The output of the second maximum pooling layer is flattened and input into a fully connected network with one hidden layer with 40 nodes. The network is trained over 30 epochs.
2) Transfer Learning. Incorporates real data into the training and updates the CNN operator calculated by CNN Training. The convolutional and pooling layers are frozen, while the real wells and seismic data are used to update the weights of the fully connected part of the network. Figure 7 shows the training network (upper panel), transfer learning network (middle panel), and validation (bottom panel) applied to Well 4. The statistics show an increase in the metrics with transfer learning and validation, when compared to the trained network. The real log is in blue and the predicted is in orange.
3) Apply to Volume. Applies the trained network (after transfer learning) to the full seismic data volume. The output volumes include the most likely class, the probability of the most likely class and the probabilities for each individual class.
4) Uncertainty Analysis. Assesses the performance of a trained Convolutional Neural Network (CNN) by systematically omitting individual wells, and then generating multiple CNN models and predictions. This process produces volumes of mean and standard deviation values, helping to identify target areas where the predictions are more reliable.

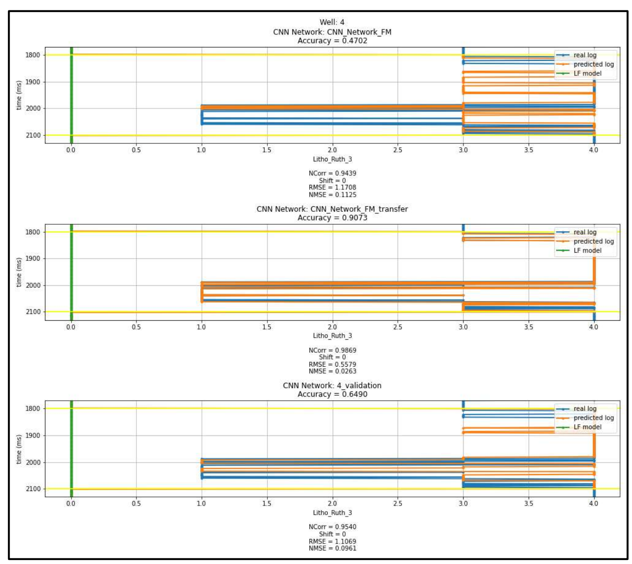

***Figure 7** – Transfer learning results QC on Well4. Training result (top panel), transfer learning result (middle panel) and validation result (bottom panel). The statistics show an improvement in the metrics with transfer learning and validation. The real log is displayed in blue and the predicted log is displayed in orange.*

Results

Table 1 shows the confusion matrix after performing the facies classification in the three test (blind) wells. This table was created with well log information and pseudo-logs of the most probable facies at the well position, between the Green and Blue horizons. In this table, the rows represent the actual class and the columns represent the predicted class.

***Table 1** – Confusion matrix from wells 1, 2, and 3 – blind wells.*

		Predicted		
		Class 1	Class 2	Class 3
Actual	Class 1	8	1	3
	Class 2	15	6	49
	Class 3	8	8	152

As we saw in Figure 2, this is a problem of unbalanced facies distribution. From Table 1, there are 12 samples in Class 1 (Pay), 70 samples in Class 2 (Wet Shaly Sand) and 168 samples in Class 3 (Shale). Class 1 was correctly predicted in 66% of the samples, 8% of the Class 1 samples were misclassified as Class 2 and 25% as Class 3. Class 2 is the most misclassified class, with 70% of samples misclassified as Class 3, 21% of samples misclassified as Class 1 and only 8% of samples correctly classified. Class 3 had 90% of the samples correctly classified.

Figure 8 shows the most probable facies over an arbitrary line passing through all the wells. The wells are overlaid, with the facies log displayed as a color block. The blind wells are highlighted in dashed black. The facies distribution is geologically consistent and matches with well logs.

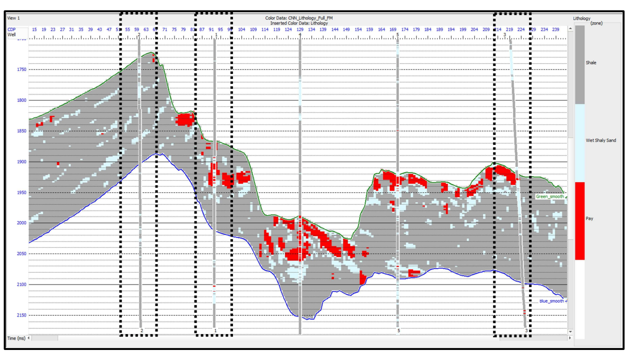

***Figure 8** – Most probable facies. The wells are overlaid with the facies log. The blind wells are highlighted in dashed black.*

Figure 9 shows the probability of the Pay facies. The comparison with the most probable facies in Figure 8 shows that there is a high probability of Pay facies in nearly all Pay classified locations. The wells are overlaid with the facies log. The blind wells are highlighted in dashed black.

Figure 10 shows the uncertainty analysis. The upper panel shows the mean of probability of Class 1 and the bottom panel the standard deviation of probability of Class 1. Higher probability in the mean and lower probability in the standard deviation shows confidence in the results. The wells are overlaid with the facies log. The blind wells are highlighted in dashed black.

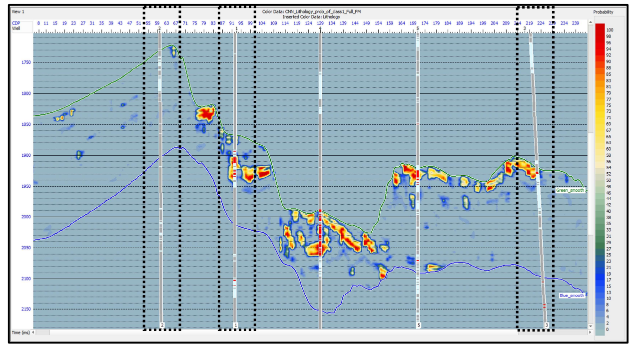

***Figure 9** – Probability of the Pay facies. The wells are overlaid with the facies log displayed as a color block. The blind wells are highlighted in dashed black.*

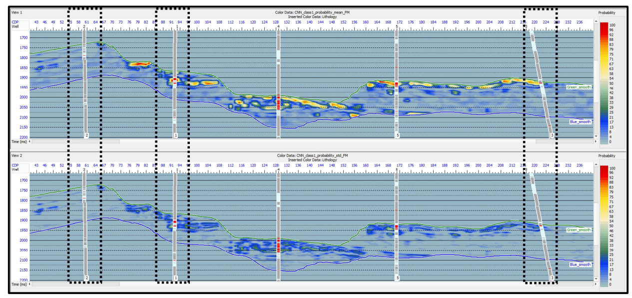

***Figure 10** – Uncertainty analysis. Mean of probability of Class 1 (upper panel) and the standard deviation of probability of Class 1 (bottom panel). The wells are overlaid with the facies log. The blind wells are highlighted in dashed black.*

Figure 11 shows a slice of the most probable facies over the Green horizon plus 10 milliseconds. Distribution of Pay facies is consistent and some areas with Pay can be evaluated as potential exploration areas. The wells are indicated, as well as the arbitrary line shown in previous figures.

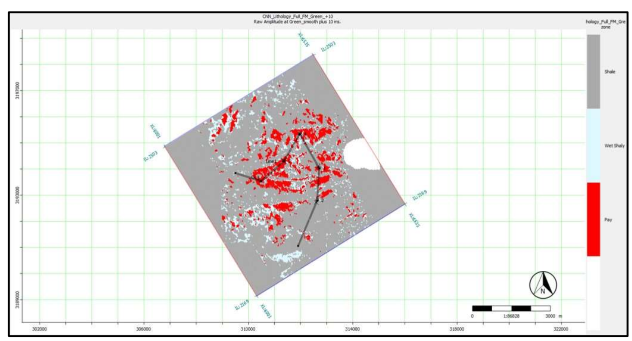

***Figure 11** – Slice of the most probable facies over the Green horizon plus 10 milliseconds. The wells and arbitrary line are indicated.*

Conclusions

We performed facies prediction in a field in the Gulf of Mexico using convolution neural networks trained on a synthetic catalog. Synthetic well data were generated by systematically varying reservoir properties and predicting elastic properties through rock physics models calibrated to two wells. We modified reservoir properties such as porosity, reservoir layer thickness, and water saturation, creating a diverse set of synthetic wells used to train a CNN model for lithology classification from seismic data. The CNN model, initially trained on synthetic data, was fine-tuned using data from just two real wells with transfer learning. This refinement improved the model's ability to accurately capture local geological features, which was validated by agreement with classifications from three blind wells. Prospective areas with Pay facies can be investigated as zones of interest. The resulting validation and uncertainty analysis give confidence regarding this approach which also can be used for quick reconnaissance.

Acknowledgments

The authors wish to thank Talos Energy for permission to show these data. We also thank GeoSoftware and the HampsonRussell developers for their support.

References

Allo, F., 2019. Consolidating rock-physics classics: A practical take on granular effective medium models: The Leading Edge, 38, no. 5, 334–340.

Allo, F., Coulon, J. P., Formento, J. L., Reboul, R., Capar, L., Darnet, M., ... & Stopin, A., 2021. Characterization of a carbonate geothermal reservoir using rock-physics-guided deep neural networks. The Leading Edge, 40(10), 751-758.

Bekti, R. A., 2020. Deep machine learning application for supervised facies classification. In EAGE/AAPG digital subsurface for Asia Pacific conference. European Association of Geoscientists & Engineers.

Colwell, T., 2022. Rock-Physics and Convolutional Network Based Approach for Property Predictions. In Second EAGE Subsurface Intelligence Workshop (Vol. 2022, No. 1, pp. 1-5). European Association of Geoscientists & Engineers.

Downton, J.E, Collet, O., Hampson, D.P, Colwell, T., 2020. Theory-guided data science-based reservoir prediction of a North Sea oil field. The Leading Edge, October, 742-749.

Downton, J., Kurian, R., Holden, T., Ibrahim, M., Hampson, D., 2022. Predicting Unconventional Shale Reservoir Properties from Seismic and Well Data Using Convolutional Neural Networks.

Dvorkin, J., and A. Nur, 1996. Elasticity of high-porosity sandstones: Theory for two North Sea data sets: Geophysics, 61, no. 5, 1363–1370.

Hashin, Z., and S. Shtrikman, 1963. A variational approach to the theory of the elastic behavior of multiphase materials: Journal of the Mechanics and Physics of Solids, 11, no. 2, 127–140.

Mayall, M. J., Yeilding, C. A., Oldroyd, J. D., Pulham, A. J., and Sakurai, S., 1992. Facies in a shelf-edge delta – An example from the subsurface of the Gulf of Mexico, Middle Pliocene, Mississippi Canyon, Block 109. AAPG Bulletin v. 76, No.4, 435-448.

Malik, J., Dixit, H. K., 2022. Application of rock physics driven deep machine learning for hydrocarbon exploration. Geohorizons, 27, 2, 118-128.

Pendrel, J., Schouten, H. J., 2020. Facies – the drivers for modern inversions. The Leading Edge, 39, 102-109.

Xu, M., Zhao, L., Gao, S., Zhu, X., Geng, J., 2022. Joint use of multiseismic information for lithofacies prediction via supervised convolutional neural networks. Geophysics, 87(5), M151-M162.